
Process parameter selection for production of stainless steel 316L using efficient multi-objective Bayesian optimization algorithm

Timur Chepiga *¹

Abstract

In this study parameter optimization for laser powder bed fusion (L-PBF) process was investigated. Using state-of-the art multi-objective Bayesian optimization (MOBO) the set of most promising process parameters (laser power, scan speed, hatch distance, etc.) was established which would yield parts with desired hardness and porosity. Gaussian process surrogate model was build on 57 empirical data points and through efficient sampling in the design space; we were able to obtain Pareto optimal solution in just 6 iterations. This greatly reduces number of experiments thus saving time and resources. The candidate process parameters prescribed by model, were experimentally validated and tested.

1. Introduction

Metal additive manufacturing (AM¹) is a sub-field of AM that focuses on production of fully functional metallic parts with complex geometry that are hard to create using conventional methods. The range of application for metal AM spreads from aerospace (Liu et al., 2017) to biomedical industries (Gebhardt et al., 2010). With recent technological advancements it is possible to create jet engine parts (Pollock, 2016), medical instruments (Culmone et al., 2019), bone implants (Sundseth & Berg-Johnsen, 2013), energy storage elements (Zhang et al., 2017) and more. However, there are several challenges hampering widespread industrial adoption one of which is lack of quality consistency and repeatability of the produced parts (DebRoy et al., 2018). Surface quality, porosity as well as other defects remain as a serious issue that can compromise performance of the produced part (du Plessis et al., 2020). Excessive amount

of pores and inclusions can lead to unacceptable strength, ductility, and fatigue resistance(Voloskov et al.). Ensuring reliability and quality of metal AM products will potentially lead to high-volume production breaking its niche market barrier.

Many defects and imperfections could be avoided beforehand by carefully setting process parameters (Zhang et al., 2020; Arisoy et al.; Kumar et al.; Kuzminova et al.). Key process parameters in laser assisted powder bed fusion (L-PBF) are laser power (P), scanning speed (v_s), hatch distance (h) and scanning strategy (Liverani et al., 2017). Together, they determine temperature gradients, solidification rate, morphology of grains (Han et al.; Kawasaki et al.) and their growth pattern affecting the microstructure of the finished part (DebRoy et al., 2018). For instance, the cooling rate of the alloy could be reduced by applying high power P and low scanning speed v_s . When insufficient heat is applied, there is not enough energy to totally melt the powder particles. As a result particles of solid powder tend to adhere to the build's surfaces resulting in "balling phenomena"(Gu & Shen).

One of the most commonly used metrics to compare parts manufactured with L-PBF under different set of processing conditions is volumetric energy density (VED) (Cherry et al.). Which is defined as :

$$E = \frac{P}{v_s \times h \times t} \quad \left[\frac{J}{mm^3} \right] \quad (1)$$

where P is laser power [W], v_s is scanning speed [mm/s], h is hatch spacing [mm] and t is layer thickness [mm]. It should be noted that Equation (1) has limitations. For instance it can not capture complex melt pool dynamics (Bertoli et al., 2017) and transition from conduction to "key-hole mode" (King et al., 2014). However, for preliminary analysis and small operating windows it serves as a good metric.

Selecting process parameters by trial and error is costly and time consuming procedure. More efficient way of choosing right configuration from prior experiments involves Bayesian methods (Shahriari et al., 2016; Gongora et al., 2020; Aboutaleb et al., 2017; Burger et al., 2020). Previous

¹Skolkovo Institute of Science and Technology, Bolshoy Blvd. 30, Bldg. 1, Moscow 121205, Russia. Correspondence to: Timur Chepiga <Timur.Chepiga@skoltech.ru>.

studies showed the applicability of the machine learning (ML) methods for optimization in L-PBF process (Ye et al.; Tapia et al., 2016; Rankouhi et al., 2021). However, they were primarily focusing on adjusting two process parameters - laser power and scanning speed, while keeping other parameters unchanged. This study builds upon and broadens previous works not only by considering more process parameters, but also by simultaneously optimizing several physical properties like hardness and porosity.

Multi-objective Bayesian optimization (MOBO) is common approach used for satisfying multiple goals and design constraints (Bradford et al.; Belakaria et al.). One of the most recent MOBO algorithms is Diversity-Guided Efficient Multi-Objective Optimization (DGEMO) (Lukovic et al., 2020) that performs well on benchmark problems showing significant advantage over similar methodologies by having nice trade-off between exploration and exploitation. The working principle of DGEMO is two-fold: first, building surrogate model of black-box objective function based on empirically obtained data; second, an acquisition function samples points in the design space that are closest to Pareto optimal. A point is said to be Pareto optimal if advancements in one objective can only be reached if at least one other objective value is decreased. The improvement of the Pareto front is estimated with a hypervolume indicator (Zitzler & Thiele, 1999), i.e., a volume of the region of the performance space populated by the points on the Pareto front. Therefore, algorithm aims to find the Pareto front with the largest possible hypervolume indicator. The acquisition function with a high exploration ratio may systematically explore the design space and prevent premature convergence of the optimization results as opposed to getting the lowest objective function value from the machine learning model through interpolation. More detailed information about underlying mathematical formulations can be found in (Lukovic et al., 2020).

2. Methodology

The Bayesian approach in this paper seeks to effectively identify the ideal process parameters for creating high-density SS 316L, such as laser power, scanning speed, hatch spacing (distance between successive laser tracks). The proposed Bayesian framework includes creating the initial input-output dataset, using the iterative process, and obtaining the ideal process parameters, as illustrated in Figure 1. Hardness and porosity are utilized as the output of initial dataset. These data entries are used during the iterative process, which includes the following steps: (1) training Gaussian process(GP)-based surrogate model on the subset of data. Mapping relationship between input variables (process configuration) and target variables (hardness and porosity); (2) Approximation of the Pareto front; (3) Selection of the next set of candidate configuration; (4) Bayesian update of the evaluated samples after which we return to the step one. This continues until we are satisfied with results or convergence is reached

of the next set of candidate configuration; (4) Bayesian update of the evaluated samples after which we return to the step one. This continues until we are satisfied with results or convergence is reached

2.1. Gaussian process

For each objective function(hardness and porosity) Gaussian process regression (GPR) model is build separately. The GPR predefines a prior Gaussian distribution with mean μ and covariance k over the regression function f without a parametric form:

$$f \sim GP(\mu, k) \quad (2)$$

The goal is to utilize the function f to build the relationship between the process parameters x and objective function Y :

$$Y = f(x) + \varepsilon \quad (3)$$

In this paper, the predictors x is the SS 316L sample manufacturing conditions, which include laser power, scanning speed, hatch spacing and others were varied in certain range Table 1 and ε is the random noise.

Table 1. Process parameter range

Parameters	Minimum value	Maximum value
Time, [min]	1	4
Gas circulation speed, [m/s]	1.5	4
Laser power, [W]	30	175
Scan speed, [mm/s]	100	3000
Hatch distance, [μm]	40	120
Scan angle, [degrees]	0	150

Using covariance function k (e.g., Matern kernel function), GPR provides a sense of similarity between the fabrication conditions as a prior. As a result, more comparable porosity and hardness values result from closer manufacturing conditions, increasing the prediction power of the GP-based surrogate model.

Training data consists of multiple manufacturing conditions (x_1, x_2, \dots, x_6) and random variables f of porosity and hardness values following a multivariate Gaussian distribution to predict the fabrication conditions and corresponding objective function values. Prior distribution of GP:

$$f(x) \sim \mathcal{N}(m(x), k(x, x)) \quad (4)$$

For the purpose of this work I have used mean function $m(x) = 0$ and different values for Matern kernel function which is known to be generalization of the squared-exponential kernel (Rasmussen & Williams).

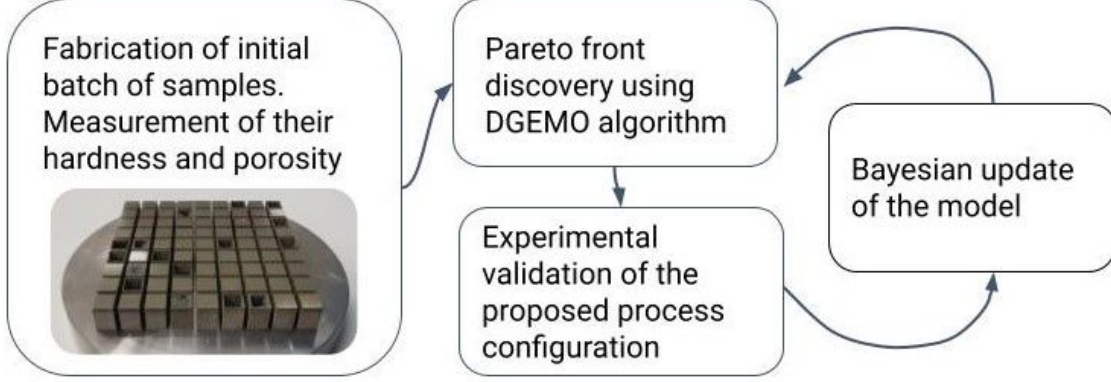


Figure 1. The workflow pipeline designed to find set of most optimal process parameters using DGEMO

I've trained GP posterior to refine the prior model by maximizing the log marginal likelihood $\log p(y|x, \theta)$ on the available dataset X, Y , where θ denotes the parameters of the kernel function. Finally, the posterior distribution of GP is given in the form:

$$f(\mathbf{x}) \sim \mathcal{N}(\mu(\mathbf{x}), \Sigma(\mathbf{x})), \quad (5)$$

where the mean function is $\mu(\mathbf{x}) = m(\mathbf{x}) + \mathbf{k}\mathbf{K}^{-1}\mathbf{Y}$, and covariance function $\Sigma(\mathbf{x}) = k(\mathbf{x}, \mathbf{x}) - \mathbf{k}\mathbf{K}^{-1}\mathbf{k}^T$, with $\mathbf{k} = k(\mathbf{x}, X)$ and $\mathbf{K} = k(X, X)$.

To better explore the Pareto front based on this surrogate model, Pareto front approximation algorithm makes use of the Jacobian and Hessian of the GP prediction $\mu(\mathbf{x}), \Sigma(\mathbf{x})$ w.r.t. x .

2.2. Bayesian optimization. Pareto front approximation

To determine the lowest predicted porosity and hardness value and its matching manufacturing condition, we use a sequential design approach with Bayesian optimization. This optimization approach lowers the costly L-PBF fabrications and seeks the global optimum in constrained design space with the fewest possible iterations.

After constructing a surrogate model G_j for each objective function f_j , we simply utilize the mean function of GP posterior as an acquisition function $\bar{f}_j = \mu_j$. The next step of our algorithm then is to compute the Pareto front over all \bar{f}_j . The Pareto front approximation, in summary, executes an iterative process with three key components. To avoid local minima and strike a balance between exploration and exploitation of the design space neighborhoods, a stochastic sampling strategy is first employed to produce a collection of random samples $x_i \in \mathcal{X}$ altered from the best samples discovered thus far. In the second stage, a local optimization technique is put into effect, leading each sample x_i to a local Pareto-optimal solution x_i^* . Different optimization

directions are explored to cover diverse regions of the Pareto front. Finally, a first-order approximation of the Pareto front is extracted around x_i , resulting in a dense set of solutions.

2.3. Bayesian update procedure. Batch selection strategy

Our method is based on two criteria: diversity and hypervolume improvement. Our diversity metric combines information from both the design and performance domains, with the goal of evenly distributing selected samples throughout diversity areas. This metric thus encourages the investigation of various parts of the Pareto front while also taking into account diversity in the design space. It is especially crucial in the early iterations when the model's uncertainty is considerable and hypervolume improvement is frequently wrong. It also keeps the optimization from falling into local minima and overly focusing on one high-performing area while ignoring other potentially promising areas.

Our selection technique tries to optimize hypervolume improvement while requiring samples to be drawn from as many different places as possible. These instructions can be written in the following format:

$$\begin{aligned} & \underset{X_B}{\operatorname{argmax}} \text{HVI}(Y_B, \mathcal{P}_f) \\ \text{s.t. } & \max_{1 \leq i \leq |\mathcal{D}|} \delta_i(X_B) - \min_{1 \leq i \leq |\mathcal{D}|} \delta_i(X_B) \leq 1 \end{aligned} \quad (6)$$

where $X_B = \{x_1, \dots, x_b\}$ is a set of b samples in a batch, $Y_B = \{\bar{f}(x_1), \dots, \bar{f}(x_b)\}$, \mathcal{P}_f is the current Pareto front, \mathcal{D}_i are linear subspaces of diversity regions, functions $\delta_i()$ are defined for each region $\mathcal{D}_i \in \mathcal{D}$ as a number of elements x_j from X_B that belong to the region \mathcal{D}_i .

The optimization issue outlined in Eq(6) can be resolved combinatorially. It would, however, need a lot of computation. We take a greedy strategy instead. Algorithm first

choose a point x_1 with the biggest hypervolume improvement, add x_1 to the batch, and then add $\bar{f}(x_i)$ to the current Pareto front \mathcal{P}_f . After that, we look for the subsequent point that has the greatest hypervolume improvement and does not reside in the same area as x_1 . Until all regions are covered, we repeat this process while avoiding all the regions from which the points were previously chosen. Algorithm resets the covered areas counter and carry out the same procedure once again if additional points are still required for the batch.

3. Case study

The stainless steel powder Höganäs AB 316L was used in this experiment with average size of the particle $30 \mu\text{m}$. The detailed powder properties are presented in (Kuzminova et al.).

For the purpose of the study 636 specimens were successfully printed with geometry of $8.0 \times 8.0 \times 10.0 \text{ mm}^3$. Production of the specimens was carried out using the metal 3D printer Trumpf Truprint 1000 realizing the L-PBF technology. The following printing parameters were varied in the limits (see Table 1) chosen according to the printer technical limits and possibility to build the solid parts: time delay between successive layers [min], argon gas circulation speed [m/s], laser power [W], scanning speed [mm/s], hatch spacing [μm] and scan strategy, which defines angle of rotation of scanning path for each successive layer. The laser beam diameter and layer thickness were constant, which were $55 \mu\text{m}$ and $20 \mu\text{m}$, correspondingly. The fabricated samples are shown in Figure 2. Note that even the precise choosing of the printing parameter limits according to the documentation provides the unprinted samples (as can be seen in Figure 2).



Figure 2. Batch of specimens printed under different processing conditions.

All printed samples were polished for the further optical porosity analysis according to the ASTM E 1245. The analysis was conducted using the an optical microscope Zeiss Axio Scope.A1 and Thixomet Pro software which converted images to grayscale. The ratio of numbers of black to white pixels was calculated to give the final porosity estimation. The fact that optical microscopy can only assess 3D porosity as an area fraction in a specific 2D plane is a significant disadvantage. As a result, this method cannot be used to estimate the pores volume accurately. For a more precise measurement of the porosity of an entire specimen, the Archimedes method is recommended (Slotwinski et al.). However, it takes more time and requires extra machining procedures, such as electrical discharge machining, to remove specimens from the substrate.

The microhardness values were obtained using a Vickers microhardness testing machine ITV-1-AM (Metrotest, Russia) according to ISO 22826. The microhardness of each cube was tested at three distinct points under a weight of 0.3 kgf.

To demonstrate how quickly proposed framework can reach the optimal solution only portion of experimental data was used to train the model. The big advantage of GP is that it can learn from small batch of data and sequentially improve with Bayesian update. In this regard we shuffled 636 data entries and took first 57 rows for model training. Based on this data, acquisition function suggests next batch of candidate samples for evaluation. To speed up research efforts, open-source automated optimal experiment design (AutoOED) was used (Tian et al., 2021). This package includes DGEMO as well as other state-of-the art MOBO algorithms.

4. Results

As evident from (Fig. 3a) sufficient VED 128.12 J/mm^3 , produces part with porosity 0.65% . In contrast, low VED 48.23 J/mm^3 (Fig. 3b) resulted in components porosity 5.27% . The Figure 4 shows the target variables as a function of VED. It is clear that optimal process configuration lies in the range between $65-280 \text{ J/mm}^3$

The obtained results concurs with previous works (Cherry et al.; Kamath et al., 2014; Bertoli et al., 2017). The operating window ranges quite widely. For instance the laser power goes from 51.5 to 159 W and corresponding scanning speed is in the range 335-1128 mm/s. In addition, the process configuration for most optimal hardness does not always coincide with the configuration for lowest porosity.

Hypervolume indicator Figure 5 demonstrates the actual advancements of Pareto front over iterations of the optimization algorithm. Proposed process configurations were experimentally validated. The Figure 5 shows scatter plot of two objective functions evaluated experimentally shown

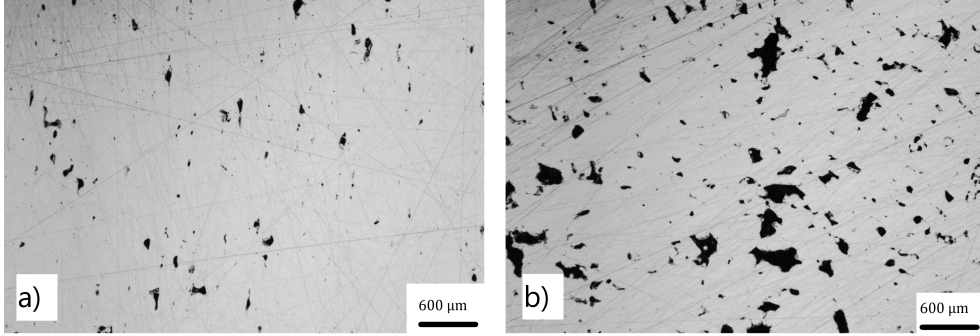


Figure 3. The optical image of the printed samples (a) sample with energy density 128.12 J/mm³ (b) sample with energy density 48.23 J/mm³

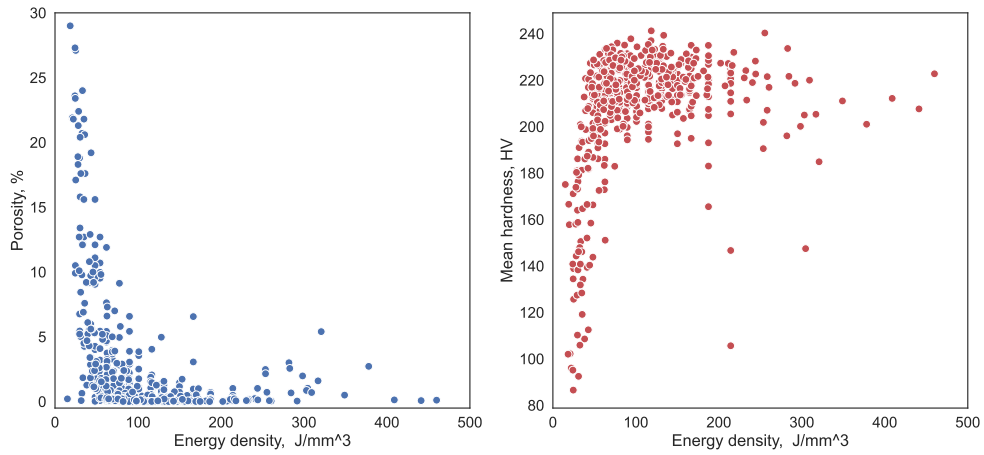


Figure 4. The scatter plot of porosity [%] and hardness [HV] as a function of VED.

in blue and Pareto front colored in red obtained after six iterations of algorithm.

5. Discussion

The rate of convergence toward Pareto front is highly depends on the initial dataset. The closer sampled points are to Pareto front Figure 5a. the faster algorithm will converge. Therefore, for the given problem it is best to leverage previous knowledge or domain expertise to select batch of points that are as close to Pareto front as possible. The laser power, scan speed and hatch distance appear to play significant role. It should be noted that proposed method can not take into account feedstock-induced defects, but rather alleviate process-induced defects for SS 316L powder.

It is evident that after just 6 iterations hypervolume indicator has risen by 9% Figure 5b. This increase indicates that a significantly wider range of performance characteristics may be achieved by further improving the existing set of process conditions. The specimens in Pareto set vary in hardness from 225 to 232 HV. The highest hardness was obtained

with power 58 W, scanning speed 257 mm/s, and hatch spacing 47 µm. Porosity of optimal solutions spans from 0.2 to 0.37%.

Applying the established Bayesian framework to the process optimization of L-PBF manufactured SS 316L samples has a number of advantages. It first minimizes the number of tests required to identify the ideal manufacturing conditions. Bayesian framework works with fewer fabrications than the complete factorial design, which tests all possible combinations of process parameters. For instance, twenty-five tests are required for a complete factorial design with five levels of laser power and scanning speed. If more components are included, the full factorial design might lead to exponentially more trials. There is no need to conduct expensive tests to cover all possible combinations of process parameters since the framework focuses on the regions that may comprise the best condition based on the Pareto approximation. The sustainability of our work may be a significant advantage. The approach is primarily concerned with conserving the resources that are used in experiments, such as time, energy, and materials.

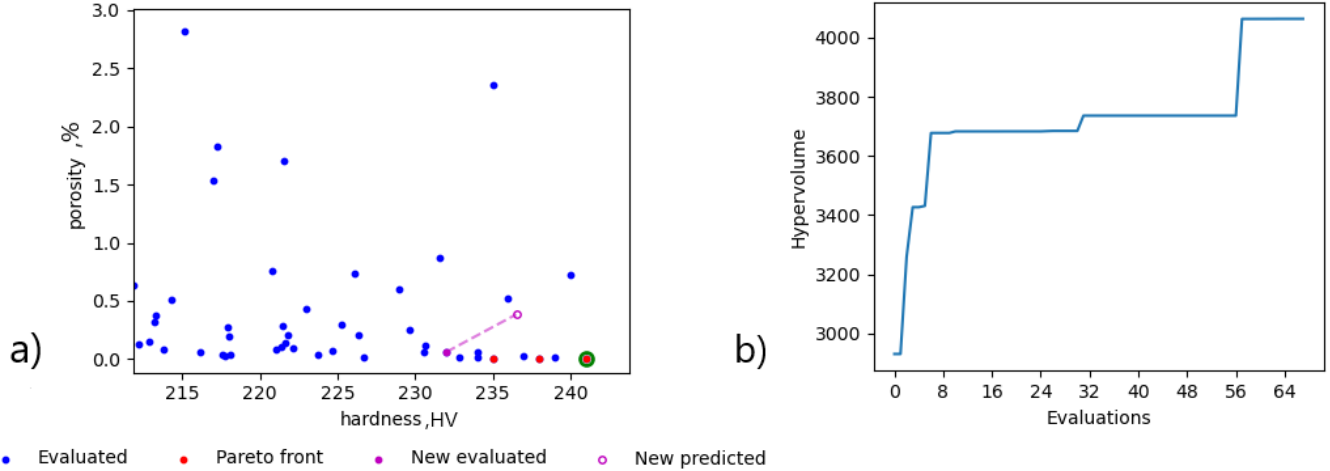


Figure 5. Performance results. (a) The scatter plot of hardness versus porosity (Pareto front is colored red) open magenta marks represents candidate configuration and solid magenta marks denotes suggested configuration after evaluation. (b) Hypervolume improvement plot on the right represents advancements toward Pareto front.

Other process design consideration could be improved. For instance if we would like to increase the buildup rate we might add another objective function that searches for high quality components that took least amount of time to build. But in order to produce AM components quickly, the scanning speed might be increased. However, this will result in elongation of molten pool and, depending on the scanning speed, the liquid pool may become unstable due to the fragmentation of the single molten pool into discrete puddles of liquid, which causes a discontinuity in the geometry and non-uniform thickness of the deposit.

Increasing the layer thickness is another way for shortening the build time. However, this will affect the surface roughness and cause additional post processing steps. We suggest the following future work for process optimization of L-PBF:

1. Dimensionality reduction and feature engineering. Extracting useful features from physical laws. Augmenting data-driven approach with mechanistic models.
2. Printing testing coupons for different kinds of mechanical testing like tensile, fracture, fatigue, creep, impact, etc. Optimization of multiple conflicting objectives like strength and ductility.
3. Employing shape and geometry information (Popov et al.) as a features for model training. Printing more sophisticated shapes to asses the generalizability of proposed method to complex geometry with different thermal gradients and solidification rates.
4. Testing different model parameters, i.e. different kernel

functions, model coefficients, acquisition functions on the same or wider dataset. Leveraging previous works (Aboutaleb et al., 2017) and material databases. Or trying out different ML models such as XGBoost(Chen & Guestrin; Karamov et al.).

5. Developing high-throughput automated experimentation (Gongora et al., 2020) for L-PBF process.

6. Conclusions

In this study novel MOBO algorithm was applied for process optimization of the L-PBF process. The proposed method extends previous works (Ye et al.; Tapia et al., 2016) by considering several process parameters and obtaining components that satisfy several objective functions. This approach is expected to be useful in creating the operating condition requirements to obtain high-density ($> 99\%$) components. The present work develops an optimal processing window that produce SS 316L effectively and affordably. A thorough analysis of porosity and microstructure after fabrication of the parts with suggested by algorithm parameters revealed several findings that are listed below:

- Model trained on relatively small batch of data has quickly found 3 points on Pareto front in just 6 iterations.
- The highest value of hardness obtained empirically was 241.3 HV corresponding to VED 118.5 J/mm^3 , with power 133 W, scanning speed 850 mm/s and hatch spacing $66 \mu\text{m}$.

- The highest relative density part had porosity 0.0007% and the following parameters: VED 119.72 J/mm³, power 108 W, scanning speed 465 mm/s, hatch spacing 97 μm.
- The VED that was explored by algorithm lies in the range of 240–265 J/mm³ hardness of produced parts were 224 – 235 HV and porosity in range 0.2 – 0.37%.

References

- Aboutaleb, A. M., Bian, L., Elwany, A., Shamsaei, N., Thompson, S. M., and Tapia, G. Accelerated process optimization for laser-based additive manufacturing by leveraging similar prior studies. *IIE Transactions*, 49:31–44, 2017. ISSN 24725862. doi: 10.1080/0740817X.2016.1189629/SUPPL_FILE/UIIE_A_1189629_SM5861.PDF. URL <https://www.tandfonline.com/doi/abs/10.1080/0740817X.2016.1189629>.
- Arisoy, Y. M., Criales, L. E., Öznel, T., Lane, B., Moylan, S., and Donmez, A. Influence of scan strategy and process parameters on microstructure and its optimization in additively manufactured nickel alloy 625 via laser powder bed fusion. doi: 10.1007/s00170-016-9429-z.
- Belakaria, S., Deshwal, A., Jayakodi, N. K., and Doppa, J. R. Uncertainty-aware search framework for multi-objective bayesian optimization. 34(06):10044–10052. doi: 10.1609/aaai.v34i06.6561.
- Bertoli, U. S., Wolfer, A. J., Matthews, M. J., Delplanque, J. P. R., and Schoenung, J. M. On the limitations of volumetric energy density as a design parameter for selective laser melting. *Materials Design*, 113:331–340, 1 2017. ISSN 0264-1275. doi: 10.1016/J.MATDES.2016.10.037.
- Bradford, E., Schweidtmann, A. M., and Lapkin, A. Efficient multiobjective optimization employing gaussian processes, spectral sampling and a genetic algorithm. 71 (2):407–438. doi: 10.1007/s10898-018-0609-2.
- Burger, B., Maffettone, P. M., Gusev, V. V., Aitchison, C. M., Bai, Y., Wang, X., Li, X., Alston, B. M., Li, B., Clowes, R., Rankin, N., Harris, B., Sprick, R. S., and Cooper, A. I. A mobile robotic chemist. *Nature* 2020 583:7815, 583:237–241, 7 2020. ISSN 1476-4687. doi: 10.1038/s41586-020-2442-2. URL <https://www.nature.com/articles/s41586-020-2442-2>.
- Chen, T. and Guestrin, C. XGBoost. In *Proceedings of the 22nd ACM SIGKDD International Conference on Knowledge Discovery and Data Mining*. ACM. doi: 10.1145/2939672.2939785.
- Cherry, J. A., Davies, H. M., Mehmood, S., Lavery, N. P., Brown, S. G. R., and Sienz, J. Investigation into the effect of process parameters on microstructural and physical properties of 316l stainless steel parts by selective laser melting. 76(5-8):869–879. doi: 10.1007/s00170-014-6297-2.
- Culmone, C., Smit, G., and Breedveld, P. Additive manufacturing of medical instruments: A state-of-the-art review. *Additive Manufacturing*, 27:461–473, 5 2019. ISSN 2214-8604. doi: 10.1016/J.ADDMA.2019.03.015.
- DebRoy, T., Wei, H. L., Zuback, J. S., Mukherjee, T., Elmer, J. W., Milewski, J. O., Beese, A. M., Wilson-Heid, A., De, A., and Zhang, W. Additive manufacturing of metallic components – process, structure and properties. *Progress in Materials Science*, 92:112–224, 3 2018. ISSN 0079-6425. doi: 10.1016/J.PMATSCL.2017.10.001.
- du Plessis, A., Yadroitseva, I., and Yadroitsev, I. Effects of defects on mechanical properties in metal additive manufacturing: A review focusing on x-ray tomography insights. *Materials Design*, 187:108385, 2 2020. ISSN 0264-1275. doi: 10.1016/J.MATDES.2019.108385.
- Gebhardt, A., Schmidt, F. M., Höller, J. S., Sokalla, W., and Sokalla, P. Additive manufacturing by selective laser melting: The realizer desktop machine and its application for the dental industry. volume 5, pp. 543–549. Elsevier B.V., 2010. doi: 10.1016/j.phpro.2010.08.082.
- Gongora, A. E., Xu, B., Perry, W., Okoye, C., Riley, P., Reyes, K. G., Morgan, E. F., and Brown, K. A. A bayesian experimental autonomous researcher for mechanical design. *Science Advances*, 6, 2020. ISSN 23752548. doi: 10.1126/SCIAADV.AAZ1708/SUPPLFILE/AAZ1708_SM.PDF. URL <https://www.science.org/doi/abs/10.1126/sciadv.aaz1708>.
- Gu, D. and Shen, Y. Balling phenomena in direct laser sintering of stainless steel powder: Metallurgical mechanisms and control methods. 30(8):2903–2910. doi: 10.1016/j.matdes.2009.01.013.
- Han, J.-K., Liu, X., Lee, I., Kuzminova, Y. O., Evlashin, S. A., Liss, K.-D., and Kawasaki, M. Structural evolution during nanostructuring of additive manufactured 316l stainless steel by high-pressure torsion. 302:130364. doi: 10.1016/j.matlet.2021.130364.
- Kamath, C., El-Dasher, B., Gallegos, G. F., King, W. E., and Sisto, A. Density of additively-manufactured, 316l ss parts using laser powder-bed fusion at powers up to 400 w. *The International Journal of Advanced Manufacturing Technology* 2014 74:1, 74:65–78, 5 2014. ISSN 1433-3015. doi: 10.1007/S00170-014-5954-9. URL <https://link.springer.com/article/10.1007/s00170-014-5954-9>.

- Karamov, R., Akhatov, I., and Sergeichev, I. V. Prediction of fracture toughness of pultruded composites based on supervised machine learning. 14(17):3619. doi: 10.3390/polym14173619.
- Kawasaki, M., Han, J.-K., Liu, X., Onuki, Y., Kuzminova, Y. O., Evlashin, S. A., Pesin, A. M., Zhilyaev, A. P., and Liss, K.-D. In situ heating neutron and x-ray diffraction analyses for revealing structural evolution during postprinting treatments of additive-manufactured 316l stainless steel. 24(4):2100968. doi: 10.1002/adem.202100968.
- King, W. E., Barth, H. D., Castillo, V. M., Gallegos, G. F., Gibbs, J. W., Hahn, D. E., Kamath, C., and Rubenchik, A. M. Observation of keyhole-mode laser melting in laser powder-bed fusion additive manufacturing. *Journal of Materials Processing Technology*, 214:2915–2925, 12 2014. ISSN 0924-0136. doi: 10.1016/J.JMATPROTEC.2014.06.005.
- Kumar, P., Farah, J., Akram, J., Teng, C., Ginn, J., and Misra, M. Influence of laser processing parameters on porosity in inconel 718 during additive manufacturing. doi: 10.1007/s00170-019-03655-9. URL <https://doi.org/10.1007/s00170-019-03655-9>.
- Kuzminova, Y., Firsov, D., Konev, S., Dudin, A., Dagesyan, S., Akhatov, I., and Evlashin, S. Structure control of 316l stainless steel through an additive manufacturing. 9(4s): 551–555. doi: 10.22226/2410-3535-2019-4-551-555.
- Liu, R., Wang, Z., Sparks, T., Liou, F., and Newkirk, J. Aerospace applications of laser additive manufacturing. *Laser Additive Manufacturing: Materials, Design, Technologies, and Applications*, pp. 351–371, 1 2017. doi: 10.1016/B978-0-08-100433-3.00013-0.
- Liverani, E., Toschi, S., Ceschini, L., and Fortunato, A. Effect of selective laser melting (slm) process parameters on microstructure and mechanical properties of 316l austenitic stainless steel. *Journal of Materials Processing Technology*, 249:255–263, 11 2017. ISSN 0924-0136. doi: 10.1016/J.JMATPROTEC.2017.05.042.
- Lukovic, M. K., Tian, Y., and Matusik, W. Diversity-guided multi-objective bayesian optimization with batch evaluations. *Advances in Neural Information Processing Systems*, 33:17708–17720, 2020. URL <https://github.com/yunshengtian/DGEMO>.
- Pollock, T. M. Alloy design for aircraft engines, 2016. URL www.nature.com/naturematerials.
- Popov, D., Kuzminova, Y., Maltsev, E., Evlashin, S., Safonov, A., Akhatov, I., and Pasko, A. CAD/CAM system for additive manufacturing with a robust and efficient topology optimization algorithm based on the function representation. 11(16):7409. doi: 10.3390/app11167409.
- Rankouhi, B., Jahani, S., Pfefferkorn, F. E., and Thoma, D. J. Compositional grading of a 316l-cu multi-material part using machine learning for the determination of selective laser melting process parameters. *Additive Manufacturing*, 38:101836, 2 2021. ISSN 2214-8604. doi: 10.1016/j.addma.2021.101836.
- Rasmussen, C. E. and Williams, C. K. I. *Gaussian Processes for Machine Learning*. The MIT Press. doi: 10.7551/mitpress/3206.001.0001.
- Shahriari, B., Swersky, K., Wang, Z., Adams, R. P., and de Freitas, N. Taking the human out of the loop: A review of bayesian optimization. *Proceedings of the IEEE*, 104 (1):148–175, 2016. doi: 10.1109/JPROC.2015.2494218.
- Slotwinski, J. A., Garboczi, E. J., and Hebenstreit, K. M. Porosity measurements and analysis for metal additive manufacturing process control. 119:494. doi: 10.6028/jres.119.019.
- Sundseth, J. and Berg-Johnsen, J. Prefabricated patient-matched cranial implants for reconstruction of large skull defects. <https://doi.org/10.4137/JCNSD.S11106>, 5:JCNSD.S11106, 2 2013. ISSN 1179-5735. doi: 10.4137/JCNSD.S11106. URL <https://journals.sagepub.com/doi/full/10.4137/JCNSD.S11106>.
- Tapia, G., Elwany, A. H., and Sang, H. Prediction of porosity in metal-based additive manufacturing using spatial gaussian process models. *Additive Manufacturing*, 12:282–290, 10 2016. ISSN 2214-8604. doi: 10.1016/J.ADDMA.2016.05.009.
- Tian, Y., Konaković, M., Luković, K. L., Erps, T., Foshey, M., and Matusik, W. Autoed: Automated optimal experiment design platform. 4 2021. doi: 10.48550/arxiv.2104.05959. URL <https://arxiv.org/abs/2104.05959v1>.
- Voloskov, B., Evlashin, S., Dagesyan, S., Abaimov, S., Akhatov, I., and Sergeichev, I. Very high cycle fatigue behavior of additively manufactured 316l stainless steel. 13(15):3293. doi: 10.3390/ma13153293.
- Ye, J., Yasin, M. S., Muhammad, M., Liu, J., Vinel, A., Slvia, D., Shamsaei, N., and Shao, S. Bayesian process optimization for additively manufactured nitinol. In *2021 International Solid Freeform Fabrication Symposium*. University of Texas at Austin.
- Zhang, F., Wei, M., Viswanathan, V. V., Swart, B., Shao, Y., Wu, G., and Zhou, C. 3d printing technologies for electrochemical energy storage. *Nano Energy*, 40:418–431,

10 2017. ISSN 2211-2855. doi: 10.1016/J.NANOEN.
2017.08.037.

Zhang, W., Tong, M., and Harrison, N. M. Scanning strategies effect on temperature, residual stress and deformation by multi-laser beam powder bed fusion manufacturing. *Additive Manufacturing*, 36:101507, 12 2020. ISSN 2214-8604. doi: 10.1016/J.ADDMA.2020.101507.

Zitzler, E. and Thiele, L. Multiobjective evolutionary algorithms: a comparative case study and the strength pareto approach. *IEEE Transactions on Evolutionary Computation*, 3(4):257–271, 1999. doi: 10.1109/4235.797969.